RECENT RESULTS FROM THE MUON $(g-2)$ EXPERIMENT

B. Lee Roberts*
Department of Physics
Boston University, Boston, MA 02215

Representing the Muon $(g-2)$ collaboration[1]

ABSTRACT

The status of the muon $(g-2)$ experiment at the Brookhaven AGS is reviewed. An accuracy of 5 ppm on the μ^+ anomalous magnetic moment has been achieved and published. Data with a statistical error of about 1.5 ppm are being analyzed with a result expected in early 2001. Additional data on tape should give a statistical error of about 0.5 ppm. A data run in 2001 will permit the measurement of the μ^- anomalous magnetic moment.

*Invited talk at the SLAC Summer Institute 2000, August 2000. For the transparancies and video see: http://www.slac.stanford.edu/gen/meeting/ssi/2000b/manu_list.html

1 Introduction

Measurements of the *gyromagnetic ratios* of elementary particles have been intimately tied to the development of our understanding of subatomic physics. The gyromagnetic ratio, g, relates the spin and magnetic moment of an elementary particle through the relationship

$$\vec{\mu}_s = g(\frac{e}{2m})\vec{S}. \tag{1}$$

In the Dirac theory, the gyromagnetic ratio, or g-factor is equal to 2. Since the g-factors of spin $\frac{1}{2}$ particles are not exactly equal to 2, is convenient to define an anomalous magnetic moment

$$a = \frac{(g-2)}{2}. \tag{2}$$

The proton, neutron and other baryons have large anomalous moments, which reflect their internal structure. The electron and muon are special in that they appear to be point-like. The small anomalous moments of these two leptons are dominated by the lowest order radiative correction $\frac{\alpha}{2\pi}$, which was first calculated by Schwinger[2] in 1948. QED calculations of the electron and muon anomalies have been carried out to eight-order (with an estimate of tenth-order) by Kinoshita.[3,4]

Fig. 1. The Feynman graphs for (a) $g = 2$; and (b) the lowest order radiative correction (Schwinger term)

The electron anomalous moment is now measured to an experimental accuracy of a few parts per billion,[5] and is well described by QED calculations.[3,4] To the level of measurement, only photons and electrons contribute, and $a \simeq 1 \times 10^{-3}$. There is no evidence to date, either from g-factor measurements or e^+e^- scattering, to indicate that the electron has any internal structure.

While the g-factor of the electron has provided a testing ground for QED, the anomalous magnetic moment of the muon has provided an even richer source of information, since the contribution of heavy virtual particles to the anomaly scales with the mass of the lepton squared. In a series of three elegant experiments at CERN,[6–8] virtual muons and hadrons have been shown to contribute at measurable levels. At present there is good agreement between experiment and theory,[3,9–11] and there is no indication of any muon substructure.

The famous CERN experiments measured $\mu_\mu = [1.001\ 165\ 9230(85)]\ (e\hbar/2m_\mu)$, a precision of ± 7.3 parts per million (ppm) for a_μ. While this result tested QED to a high level, and showed for the first time the contribution of virtual hadrons to the magnetic moment of a lepton, the sensitivity was not sufficient to observe the electroweak contribution from virtual $W^\pm$ and Z^0 gauge bosons. The goal of our experiment is an overall accuracy of ± 0.35 ppm which allows sufficient sensitivity to measure the electroweak contribution, as well as to search for physics beyond the standard model.

The theoretical value of a_μ consists of contributions from QED,[3] virtual hadrons,[12–17] and virtual electroweak gauge bosons.[18–21] Taking the value of α from the electron $(g-2)$ experiment,[22] the total QED contribution is $a_\mu^{QED} = 116\ 584\ 706(2)\ \times 10^{-11}$. The QED contribution is calculated to a precision of a few parts per billion. The agreement between the calculated and measured $(g-2)$ values for the electron gives us great confidence in the QED calculation.

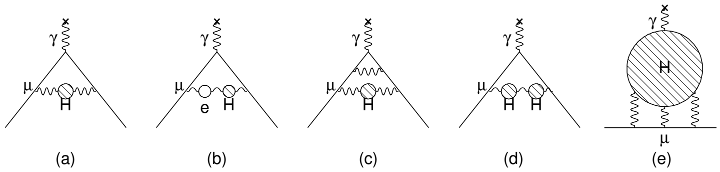

Fig. 2. Hadronic contributions to the muon anomalous moment. In these diagrams, H refers to a loop with hadrons (quarks). (a) The lowest order hadronic vacuum polarization, which is the dominant diagram.[14] (b) (c) (d) Higher order hadronic vacuum polarization diagrams.[15] (e) The light-on-light hadronic contribution.[14,17] The $\times$ indicates the virtual photon originating from the magnetic field.

Virtual hadrons contribute to the muon anomaly through vacuum polarization at a measurable level. The most important diagrams are shown in Fig. 2. The largest contribution (and the largest uncertainty) comes from the hadronic vacuum polarization diagram (Fig. 2(a)), which cannot be calculated from first principles. Instead measurements of $R(s)$, the ratio

$$R(s) = \frac{e^+e^- \to \text{Hadrons}}{e^+e^- \to \mu^+\mu^-} \tag{3}$$

are used as input to the dispersion integral

$$a_\mu^{hadronic} = (\frac{\alpha m_\mu}{3\pi})^2 \int_{4m_\pi^2}^{\infty} \frac{ds}{s^2} K(s) R(s) \tag{4}$$

where

$$K(s) = \frac{3s}{m_\mu^2}\left[x^2(1-\frac{x^2}{2}) + (1+x)^2(1+\frac{1}{x^2})\left[\ln(1+x) - x + \frac{x^2}{2}\right] + \frac{1+x}{1-x}x^2\ln x\right] \tag{5}$$

is a kinematic factor, with

$$x = \frac{1-\beta}{1+\beta}, \qquad \beta = \sqrt{1-\frac{4m_\mu^2}{s}}. \tag{6}$$

The higher order hadronic contributions (Figs. 2(b-d)) are also calculated from these data,[15] but the hadronic light-on-light contribution[16,17] (Fig. 2(e)) must be obtained from a model calculation.

The total hadronic vacuum polarization contribution is $a_\mu^{Had} = 6882(154) \times 10^{-11}$ (~ 60 ppm of a_μ), where the error is dominated by the errors on the experimental data. The total hadronic contribution is given by[14] $a_\mu(\text{had}) = 6738(70) \times 10^{-11}$ which is 57.79 ± 0.60 ppm of a_μ.

The error quoted above does not reflect recent progress in $R(s)$ measurements at Novosibirsk and BES, reported in preliminary form at the ICHEP2000 conference in Osaka. Data at center-of-mass energies between 2 and 5 GeV from BES are likely to reduce the error from that region to a negligible level. In the energy region between 0.4 and 1.4 GeV, newly analyzed data from Novosibirsk should reduce the corresponding error in a_μ to 0.29 ppm. Data from hadronic τ decays should further reduce the error in roughly the same kinematic region. Finally, the region between 1.4 and 2.0 GeV will be addressed by the VEPP-2000 project at Novosibirsk, which will raise the collider's center-of-mass energy to 2 GeV. The uncertainty on the standard model value of a_μ will likely be reduced to about $\sim \pm 0.35$ ppm in the near future.

The one-loop electroweak contributions to a_μ (see Fig. 3(a),(b)) have been available for some time.[18] Recent higher order calculations, which include both fermionic[19,20] and bosonic[21] two-loop terms, have been confirmed by an independent calculation.[23] These authors obtain second order contributions which turn out to be surprisingly large.

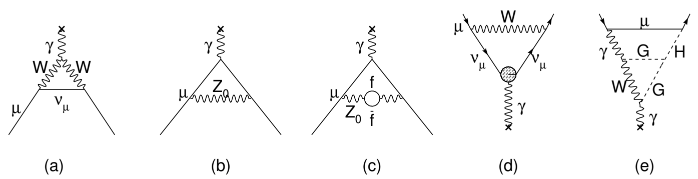

Fig. 3. Weak contributions to the muon anomalous magnetic moment. Single-loop contributions from (a) virtual W and (b) virtual Z gauge bosons. These two contributions enter with opposite sign, and there is a partial cancellation. The single-loop standard model Higgs contribution is negligible. The two-loop contributions fall into three categories: (c) fermionic loops which involve the coupling of the gauge bosons to quarks, (d) bosonic loops which appear as corrections to the one-loop diagrams, and (e) a new class of diagrams involving the Higgs where G is the longitudinal component of the gauge bosons. See reference[21] for details. The $\times$ indicates the virtual photon originating from the magnetic field.

The first order weak contribution of 195×10^{-11} is reduced to $151(4) \times 10^{-11}$ (1.3 ppm of a_μ) when the second order terms are included.

The total theoretical prediction is $a_\mu^{Theory} = 116\ 591\ 63\ (8)\ \times 10^{-10}$ where the theoretical error of ± 0.7 ppm is dominated by the uncertainty on the hadronic vacuum polarization contribution.

Theoretical interest in possible non-standard model contributions to the muon $(g-2)$ value has risen substantially in the past five years, and a great deal has been written about possible contributions to the muon $(g-2)$ value from non-standard model physics.[24,9] In Table 1 the sensitivities to several examples of new physics are given, assuming that the experimental error on a_μ is ± 0.35 ppm, and the error on the hadronic contribution is significantly less.

For example, just as proton substructure produces a g-value which is not equal to two, muon (or W) substructure would also contribute to the anomalous moment, the critical issue being the scale of the substructure.[25] A standard model value for $(g-2)$ at the 0.35 ppm level would restrict the substructure scale to around 5 TeV. If leptoquarks exist, they too could contribute to the non-standard model value of $(g-2)$.[26] The muon $(g-2)$ obtains its sensitivity to W substructure and anomalous gauge couplings through the $WW\gamma$ triple gauge vertex in Fig. 3(a). The combined sensitivity of LEP1, LEP2 and $(g-2)$, and the unique contribution which $(g-2)$ makes in constraining the existence of such anomalous couplings, is described by Renard et al.[27]

Fig. 4. The lowest order supersymmetric contributions to $(g-2)$.

Supersymmetry has become a serious candidate for physics beyond the standard model. There is a large sensitivity to almost any supersymmetric model with large $\tan\beta$ (the ratio of the vacuum expectation value of the two Higgs fields).[24] The SUSY contribution is shown in Fig. 4. In the case of large $\tan\beta$, the chargino (χ^-) diagram dominates the contribution to $(g-2)$ from SUSY, and is given by[24]

$$a_\mu(\mathrm{SUSY}) \simeq \frac{\alpha}{8\pi\sin^2\theta_W}\frac{m_\mu^2}{\tilde{m}^2}\tan\beta \simeq 140\times10^{-11}\,(\frac{100\ \mathrm{GeV}}{\tilde{m}})^2\tan\beta, \tag{7}$$

where $\tilde{m}$ is the largest mass in the loop. The goal of E821 is to reach a precision of $\pm 40\times10^{-11}$ (±0.35 ppm), so the factor of 140 in Eq. 7 corresponds to 1.2 ppm in a_μ. For $\tilde{m} = 750$ GeV and $\tan\beta = 40$, $a_\mu(\mathrm{SUSY}) = 100\times10^{-11}$, a contribution which is 2.5 times larger than the sensitivity we hope to achieve. For $\tilde{m} = 500$ GeV, the effect is 224×10^{-11} or 5.6 ppm.

Several measurements in addition to that of the muon anomalous moment will be made in our experiment. We expect to improve the limit on the muon electric dipole moment (EDM) by an order of magnitude over the current limit of $d < 3.7\pm3.4\times10^{-19}$ e-cm, which was placed by the CERN $(g-2)$ experiment. An EDM would produce a spin motion out of the plane of the storage ring, so the signal would be a change in time of the vertical position of the decay positrons on the detectors. Since this small (the standard model value for the EDM is 10^{-38} e-cm) spin motion rides on top of a very large $(g-2)$ precession, the EDM measurement from E821 will be dominated by systematic errors. To obtain much more than an order of magnitude improvement over the CERN EDM result, it will be necessary to do an optimized EDM measurement, and preliminary studies show that we might reach a sensitivity of 10^{-24} e-cm. If there is non-standard model physics such as SUSY present, the EDM would be sensitive to it.

New Physics	E821 Sensitivity	Comments
μ substructure[a]	$\Lambda \geq 5\; TeV^{\dagger}$	LHC domain
μ Form factors[b] $(1-k^2/\Lambda^2)$	$(W^{\pm})\ \Lambda > 450 GeV$ $(Z^0)\ \Lambda > 64 GeV$ $(\gamma)\ \Lambda > 180 GeV$	$\Lambda_{LEP\ I} > 300 GeV$
excited muon	$m_{\mu^*} \geq 400\; GeV$	LEPII comparable
$W^{\pm}$ substructure[c]	$\Lambda \geq 400\; GeV^{\dagger}$	LEPII $\sim 100 - 200\; GeV$
$\frac{(g_W-2)}{2} \neq 0$	$\geq 0.02^{\ddagger}$	LEPII~ 0.05, LHC~ 0.2

†Scales as the square root of the error.

‡Scales linearly with error.

[a]For substructure $\Delta a_{\mu} \sim m_{\mu}^2/\Lambda^2$.

[b]See P. Méry, S.E. Moubarik, M. Perrottet, F.M Renard, Z. Phys. **C46**, 229 (1990).

[c]Goes to 0 if $M_W \to 0$ to get proper coupling to conserved current.

Table 1. Sensitivity to new physics other than SUSY if $\sigma_{a_{\mu}} = 0.35\; ppm$ (This table is taken primarily from Kinoshita and Marciano.[9])

However, unlike $(g-2)$, the standard model contribution ($\sim 10^{-38}$ e-cm) to the EDM is negligible compared to that predicted by SUSY models, and the interpretation would not be subject to any uncertainties in our knowledge of the standard model contribution.

We will measure $(g-2)$ for both μ^+ and μ^- thus providing a test of CPT (the CERN experiment[8] obtained values for these two which differed by over one σ). The experiment also tests special relativity, since the dilated muon lifetime in the storage ring is one of the parameters which comes out of the fit to the positron time distribution.

2 The Experimental Technique

A charged particle moving transverse to a uniform magnetic field will go in a circle with the orbital cyclotron frequency

$$\omega_c = \frac{(eB)}{(m\gamma)}. \tag{8}$$

The spin precession frequency in this same magnetic field is given by

$$\omega_s = \frac{geB}{2m} + (1-\gamma)\frac{eB}{m\gamma}. \tag{9}$$

Thus the spin vector of a charged particle moving transverse to a uniform magnetic field will precess relative to the momentum vector with a frequency ω_a, which is given by the difference between the orbital cyclotron frequency ω_c and the spin precession frequency ω_s. The frequency is

$$\omega_a = \omega_s - \omega_c = \frac{e}{m} a_\mu B, \tag{10}$$

where ω_a is directly proportional to the anomalous moment and is independent of the particle's momentum.

Vertical focusing must be provided to keep the muon beam stored, which can be accomplished with magnetic multipoles, or with an electrostatic quadrupole field. However, if magnetic multipoles are used, it is difficult to determine the average B field to the accuracy needed for a precision measurement of a_μ. In a region in which both magnetic and electric fields are present, the relativistic formula for the precession is given by[28]

$$\vec{\omega}_a = \frac{d\Theta_R}{dt} = -\frac{e}{m}\left[a_\mu \vec{B} - \left(a_\mu - \frac{1}{\gamma^2 - 1}\right)\vec{\beta}\times\vec{E}\right], \tag{11}$$

where Θ_R is the angle between the muon spin direction in its rest frame and the muon velocity direction in the laboratory frame. The other quantities refer to the laboratory frame. If the muon beam has the "magic" value of $\gamma = 29.3$, then the coefficient of the $\vec{\beta}\times\vec{E}$ term is zero, and the electric field does not cause spin precession. Thus the precession of the spin relative to the momentum is determined entirely by the magnetic field, and one can use electrostatic quadrupoles for vertical focusing.

Because the muon's lifetime is relatively long, and because muons are produced fully-polarized along their direction of motion in pion decay at rest, it is possible to store large numbers of polarized muons in a storage ring. In the three-body decay $\mu^+ \to e^+\bar{\nu}_\mu\nu_e$, the highest energy positrons are preferentially emitted parallel to the muon spin direction in the muon rest frame. Also, the highest energy electrons in the muon rest frame, when emitted parallel to the muon momentum, are Lorentz boosted to become the highest energy electrons in the lab frame. Therefore, the number of high energy electrons is a maximum when the muon spin is parallel to the momentum, and a minimum when it is anti-parallel, thus making it possible to measure the spin (or anomalous) precession frequency by counting high energy electrons as a function of time. This time spectrum will show the muon lifetime modulated by the spin precession frequency.

The muon beam for storage in our storage ring is obtained from a bunched proton beam extracted from the AGS and directed onto a production target, which produces a secondary beam of charged pions. The AGS beam contains either six (1999) or twelve (2000, 2001) proton bunches ($\sigma \simeq 30ns$), with a bunch intensity limited to $\leq 7 \times 10^{12}$ protons by shock considerations in the production target. The total proton intensity in a single AGS cycle with 12-bunch operation was $\sim 60 \times 10^{12}$ protons.

The secondary beam momentum is set with dipoles and a momentum slit, and the beam is brought down a 100 m beamline which has a straight 74 m long quadrupole decay channel to collect muons from pion decay. Just upstream of the storage ring, a second momentum slit permits us to select a pion beam or, by adjusting the momentum lower by $\simeq 1\%$, a muon beam. Initially we injected pions into the ring and used the $\pi \to \mu\nu$ decay to kick the muons onto stored orbits.[10] Since the summer of 1998, we have injected muons into the storage ring, storing them with a 10 mrad magnetic kick.

With muon injection, about 10^4 muons were stored in the ring per proton bunch, and the number of detected positrons per hour was increased by an order of magnitude over the pion-injection method employed previously. Furthermore, the injection-related background (flash) in the positron detectors was reduced by a factor of about 50, since most of the pions were removed from the beam before it entered the storage ring.

The storage ring is a 600 ton, superferric magnet with 14 m diameter coils which excite the B field.[29] The ring functions as a weak focusing betatron, with a field index of 0.137. After a rigorous program of shimming, the B field uniformity is better than ± 2 ppm, integrated over azimuth. The storage ring parameters are given in Table 2.

The muon decay electrons, having lower momenta than the stored muons, are swept by the B-field into twenty-four scintillating fiber-Pb calorimeters, which are spaced evenly around the interior of the ring. The calorimeter pulses were continuously sampled by custom 400 MHz waveform digitizers (WFDs), which provided both timing and energy information for the positrons. Both the NMR (magnetic field) and WFD clocks were phase-locked to the same LORAN-C frequency signal.[30] The waveforms were zero-suppressed, and stored in memory in the WFD until the end of the AGS cycle. Between AGS acceleration cycles the WFD data were written to tape for off-line analysis, as were the calorimeter calibration data and the magnetic field data.

We measure the frequency of oscillation in the number of high energy decay electrons, which is the same as the anomalous precession frequency. In the time histogram

Fig. 5. The 700 ton muon $(g-2)$ storage ring during a maintenance period. The magnet yoke is covered with (white) thermal insulation, except at 9:00 o'clock where it is pulled back. The lighter colored inner-radius ring at 9:00 is the top cryostat for the inner-radius coil, and the bottom inner-radius cryostat can also be seen below the magnet gap at 2 o'clock. Most of the 24 electron calorimeter stations are installed. The muon kicker modulators are the three "cannon-like" objects at 1:00 o'clock. Two sets of tracks the detectors ride on can be seen to the right of the third kicker modulator, since these detectors have been removed.

of high-energy decay electrons one observes the exponential lifetime expected from muon decay, modulated by the $(g-2)$ frequency,

$$N(t) = N_0 e^{-t/\gamma\tau}(1 + A\cos(\omega_a t + \phi)), \tag{12}$$

where A, the product of the decay asymmetry and the stored muon polarization, is about 0.4 for electrons above 1.8 GeV (the maximum electron energy is 3.1 GeV). The full data set from the 1999 run is shown below in Fig. 6. Ultimately $(g-2)$ plans to collect about 2×10^{10} decay positrons with energy above 1.8 GeV, spread over more than ten time-dilated muon lifetimes (640 μs).

Parameter	Value	Comments
(g-2) Frequency	$f_a \sim 0.23 \times 10^6/s$	$\omega_a = 2\pi f_a$ $\tau_a = 1/f_a = 4.37\ \mu$ s
Muon Lifetime	$\gamma\tau = 64.4\ \mu$ s	
Muon kinematics	$p_\mu = 3.094$ Gev/c $\gamma_\mu = 29.3$	The Central Momentum = The Magic Momentum
Cyclotron Period	$\tau_{cyc} = 149$ ns	
Central Radius	$\rho = 7112$ mm — $(280'')$	
Magnetic Field	$B = 1.4513$ T	
Storage Aperture	9.0 cm circle	
In one lifetime:	432 revolutions around ring	14.7 *(g-2)* periods

Table 2. Storage Ring Parameters

In our storage ring, the magnetic field (see Eqn. 11) is a nearly pure dipole field which can be measured to a precision of a few parts in 10^7 with NMR. At the edge of the 9 cm diameter storage aperture, the quadrupole and higher multipole strengths are at the few ppm level relative to the vertical dipole field. There is a small second order correction from the electric field because the cancellation only occurs for the central momentum of the storage ring. Because of the vertical betatron motion of the stored muons, there is also a "pitch" correction[32] from the vertical betatron motion, since $\vec{\beta} \cdot \vec{B}$ is not exactly zero.

3 Beam Dynamics

A knowledge of beam dynamics is important to the ω_a analysis. The magnetic field which enters into Eq. 10 (and Eq. 11) is the magnetic field in the storage ring <u>averaged over the muon distribution</u>. Thus we need to measure the field very well, and we need to have some knowledge of the muon distribution in the ring. Furthermore, both the electric field and "pitch" corrections require some knowledge of the muon distribution. The electric-field correction, 0.5 ppm in the 1999 run, is proportional to the rms momentum spread of the stored muon beam, which we can measure by examining the rate at which the beam debunches at early times.

The $(g-2)$ storage ring functions as a weak focusing betatron,[33] with an average

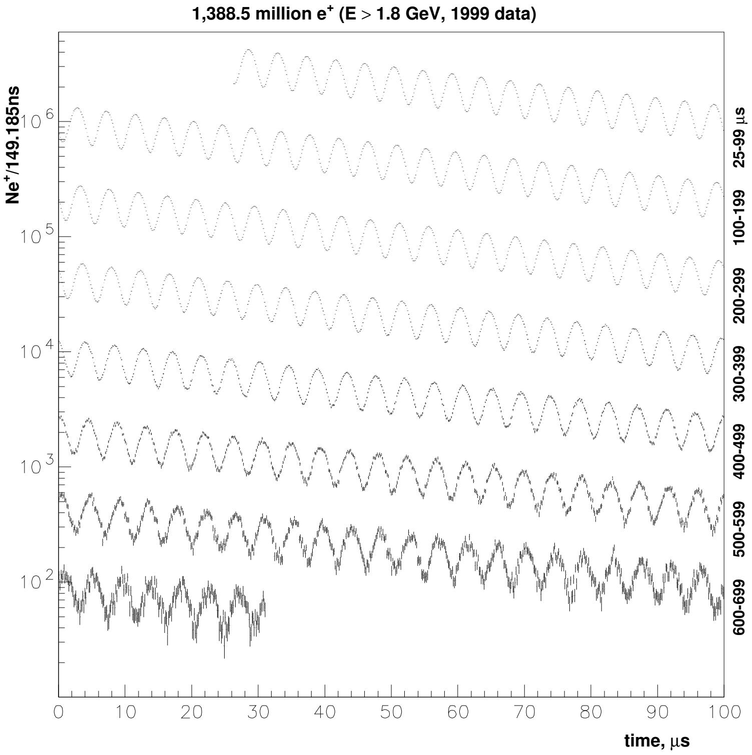

Fig. 6. The 1999 data. Because we accumulate data over many lifetimes, the time scale is folded back over every 100 μs. These data clearly show the exponential muon lifetime modulated by the spin precession.

field index $n = 0.137$. With the assumption that the vertical focusing is provided by a uniform quadrupole field spread around the storage ring, the horizontal and vertical betatron oscillations obey the equations

$$\ddot{x} + \omega_x^2 x = 0, \quad \text{horizontal (radial)} \tag{13}$$

and

$$\ddot{y} + \omega_y^2 y = 0, \quad \text{vertical,} \tag{14}$$

which are harmonic oscillator equations with the frequencies

$$\omega_x = \omega_c \sqrt{1-n}; \qquad \omega_y = \omega_c \sqrt{n}. \tag{15}$$

ω_c is the cyclotron frequency. We use the standard accelerator coordinates, x for radial position, y for vertical, and s for arc length around the ring. The point $x = y = 0$ is the center of the storage region. From Eqn. 15 one sees that the requirement for stable orbits is $0 < n < 1$.

For a uniform quadrupole gradient, the field index n is defined by

$$n = -\frac{\rho}{B_{0y}} \frac{\partial B_y}{\partial x} \tag{16}$$

where ρ is the storage ring radius, B_{0y} is the vertical dipole magnetic field, $\partial B_y / \partial x$ is the magnetic gradient term which provides the quadrupole focusing. If both magnetic and electric gradient terms are present, the effective field index becomes[34]

$$n_{\mathrm{eff}} = -\frac{\rho}{B_{0y}} \frac{\partial B_y}{\partial x} - \frac{\rho}{\beta B_{0y}} \frac{\partial E_x}{\partial x}. \tag{17}$$

In E821, only an electric field is used to provide vertical focusing with the magnetic field as pure a dipole field as possible.

Eqns. 13 and 14 represent the motion of single particles in our storage ring. An alternate way of looking at the beam motion is to view the ring as a spectrometer. With a field index of 0.137, the horizontal betatron frequency is $f_{\mathrm{rad}} = 0.93 f_C$, which means that in one betatron wavelength $\lambda_{\mathrm{rad}} = 1.075(2\pi\rho)$, the particle returns to its starting radial position. In ~ 13.3 turns, the the betatron oscillation returns to the same radial (x) and azimuthal (s) position in the storage ring. We return to this point below.

In order to deliver the beam to the edge of the storage region, an iron-free superconducting septum magnet called an inflector[35] produces a 1.5 T dipole field which opposes the main storage ring field, thus permitting the beam to arrive at the edge of the storage volume essentially undeflected. The inflector aperture is 18 mm wide and 53 mm high, and the region inside the ring available for beam storage is a 90 mm diameter circle. While this small injection aperture, which does not match the storage ring aperture, is contrary to usual storage ring practices, ordinary storage rings do not have magnetic fields uniform to a few ppm. The usual technique of a storage ring composed of separate elements is not possible here, and a hole cut into the magnet for injection would spoil the excellent field uniformity. Thus the storage ring magnet is a circular "C" dipole magnet, 14 m in diameter, with a pole gap of 180 mm.[29] The opening of the "C" faces the circle center, and the beam enters through a small hole in the magnet yoke. The geometry showing the inflector exit and the storage region between the magnet pole pieces is shown in Fig. 7.

At the inflector exit the beam is 77 mm (not 76 as is indicated in the drawing) from the center of the storage region. Since the beam will travel in a circle, without a kick it

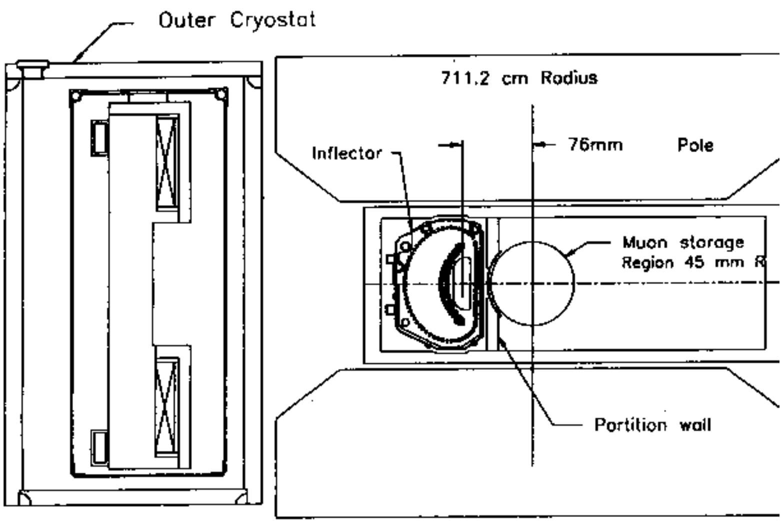

Fig. 7. An elevation view of the geometry of the inflector and the storage ring magnet. The beam vacuum chamber and the inflector cryostat are a coupled package. The chamfered pole pieces can be seen immediately above and below the inflector and storage region. The beam enters through the "backward D"-shaped aperture 77 mm (not 76 as shown) from the storage ring center. The large Xs at the top and bottom of the outer cryostat are the superconducting coils which excite the magnetic field.

will return to hit the side of the inflector and be lost. A 0.1 T-m (10 mrad) kick must be applied a quarter of a betatron wavelength after the inflector exit to place the beam at the center of the storage region. The usual kicker techniques with ferrite core magnets cannot be employed here, because of the precision magnetic field. The magnetic kick was generated with a pulsed current, which had a peak current of 4100 A and a half period of 400 ns.

Three pulse-forming networks powered three identical 1.7 m long one-loop kicker sections consisting of 95 mm high parallel plates on either side of the beam. The current pulse was formed by an under-damped LCR circuit. The kicker plate geometry and composition were chosen to minimize eddy currents. The residual eddy current effect on the total field seen by the muons was less than 0.1 ppm 20 μs after injection. The time-varying magnetic field from the eddy currents was calculated with the program OPERA[36] and was measured in a full-size straight prototype vacuum chamber with the use of the Faraday effect.[37] Since the muons circulate in 149 ns, they were kicked several times before the kicker pulse died out. Simulations show that because of the phase-space mismatch between the inflector and the storage region, a perfect kick would result in 7.5% of the beam being stored. With the actual kicker waveforms these calculations predict a storage efficiency of 6.6%. While not exactly at the level of efficiency expected in the usual accelerator application, this injection efficiency more properly should be compared with the pion injection efficiency of 3×10^{-6} muons stored per pion injected into the ring. Thus the order of magnitude improvement in stored muons and the substantial reduction in background over that obtainable with pion injection show the real success of this new technique.

During injection, and for 16 μs following injection, the electrostatic quadrupoles are powered asymmetrically, so that the beam is lifted and displaced sideways in the storage ring. This permits the beam to be scraped on circular collimators placed at several locations inside of the ring. After scraping, the quadrupole plates are returned to symmetric potentials with an RC time-constant of 5 μs.

The beam of particles enters the ring in a bunch. Since all muons are traveling at essentially the same velocity, those with larger radii will be overtaken by those at smaller radii, and the beam will debunch. This can be seen clearly in the positron time spectra from the detectors.

Fig. 8(a) shows the high energy positron time spectrum early in the data-taking cycle. The interval between the peaks is the beam's 150 ns "fast rotation" time around the storage ring. Fig. 8(b) shows the time spectrum about 30 μs later, by which time the debunching of the beam has noticeably washed out the fast rotation structure. Figure 8(c) shows the inferred equilibrium radius distribution which peaks at the radius corresponding to the magic gamma, 711.2 cm, but is not symmetric about it, having something of a high side shoulder. Two independent analyses, one using Fourier techniques, arrive at distributions which are virtually identical.

The tracking code mentioned above has also been used to calculate the average magnetic field seen by the stored muons, as well as the pitch and radial-E-field correction. The distribution of equilibrium radii calculated from tracking is overlaid with the "fast rotation analysis" (discussed below) in Fig. 8(c). The radial E-field calculation and pitch correction calculations are consistent with our expectations.

The beam exiting the inflector has a narrow waist imposed on it by the aperture of the inflector. This waist will be reformed one betatron wavelength later around the ring. In ~ 13 turns, this waist will travel around the ring. If there were no momentum dispersion in the storage ring, the waist would reform at 180° and return to the same azimuthal position every ~ 6.5 turns. In addition to the motion of this horizontal waist, the beam

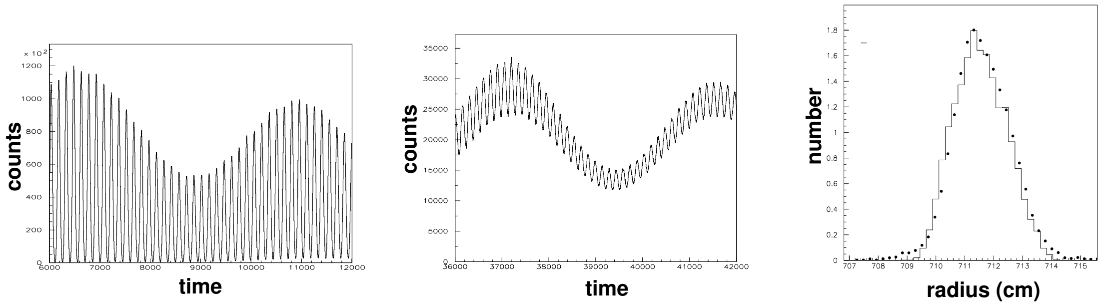

(a) (b) (c)

Fig. 8. The time spectrum of positrons at early times. The narrow structure is from the bunched beam structure, and the slower "wiggle" is from the $(g-2)$ precession. (a) Clear fast rotation structure about 6 microseconds after injection. (b) Faded fast rotation structure about 36 microseconds after injection. (c) The equilibrium radius distribution calculated using the tracking code (histogram) and obtained from an analysis of the beam debunching at early times (points) (1998 data).

oscillates coherently about the central orbit because it is not kicked perfectly. Because the positron detector acceptance varies slightly with radius, we see both the radial coherent betatron motion, and the horizontal beam waist motion around the ring, in the 1999 high-statistics data. The width variation has a clear first- and second- harmonic dependence, as would be expected from the arguments above.

These betatron motion effects were first seen in data from the scintillating fiber harps which we have as beam diagnostic tools. The harps consist of seven 0.5 mm scintillating fibers strung either radially or horizontally, and are used to sample the beam profile. The measurement is destructive and is not performed during standard data runs but still gives a very reliable idea of the beam profile for many tens of microseconds.

Data from the harps are shown in figure 9. The two data sets, with beam scraping on and off, have different characteristic frequencies but send the same message: the beam undergoes a collective radial betatron motion, here of amplitude 0.4 cm. These coherent betatron oscillations are most prominent at early times but persist for more than 100 microseconds. The oscillations arise because the kick given to the incoming beam is not perfect. Instead of arriving on a stored circular orbit centered on the middle of the storage ring, the beam describes a series of roughly circular orbits with a slowly moving center. A small radial acceptance bias transforms the oscillatory motion into a small modulation of the basic $(g-2)$ precession spectrum. The effect is small, but must be accounted for in our 1999 analysis.

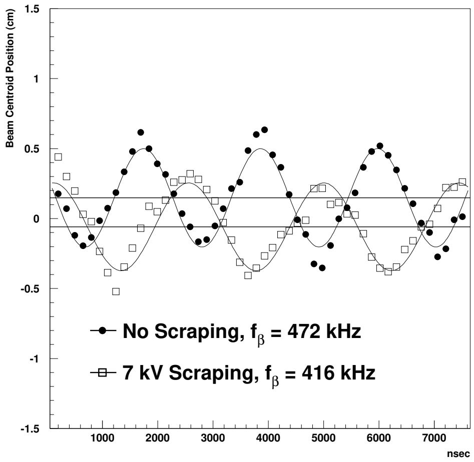

Fig. 9. Average beam radius vs. time. When the beam is first injected, the electrostatic quadrupoles are powered asymmetrically this moving the beam up and off-center horizontally, thus scraping it on collimators. This changes slightly the n-value of the weak-focusing storage ring during scraping.

4 Analysis

Experimentally, we determine the muon frequency ω_a from the detectors' positron time spectra, and the magnetic field from the proton NMR frequency ω_p (corrected to the free-proton value). From the ratio $R = \omega_a/\omega_p$ we determine

$$a_\mu = \frac{R}{(\lambda - R)} \tag{18}$$

where $\lambda = \mu_\mu/\mu_p$ is measured independently.[38,39] The analysis is done blind, meaning that for each frequency analysis (ω_a and ω_p) an arbitrary offset is put into the data, so that without knowledge of the offsets one cannot determine a_μ. Since each offset is known by only one person, it is impossible for anyone doing the analysis to determine a_μ without the collaboration of these two people. Furthermore, the four independent analyses of ω_a, and the two independent analyses of ω_p had additional offsets determined by the principals, which were removed late in the analysis process. Soon all offsets will be removed on the analysis of the 1999 data.

The heart of any precision experiment is the analysis of systematic errors. The most important errors in the analysis of the 1998 data are listed in Table 3. Limitations on our knowledge of the B-field are important. Some errors are related to the dynamics of the stored muon beam and others to the performance of the electron calorimeters and their associated PMTs, as well as to the procedures used to reconstruct the electron times and energies from the waveform record. With each new data set we have been able, thus far, to reduce the systematic errors well below the statistical errors. In the 1999 data set, the systematic errors are on the order of ~ 0.5 ppm with a statistical error of ~ 1.5 ppm.

Systematic Effect	ϵ (ppm)
1. Magnetic Field B	0.5
2. Timing Shifts	<0.1
3. Pileup	<0.6
4. Gain Changes	<0.1
5. Coherent Betatron Oscillations	0.2
6. Radial E Field, Pitch Correction	0.3
7. Backgrounds	<0.5
8. Lost Muons	<0.1
9. Fitting Start Time	0.3
10 Binning Effects	0.2
Total Systematic Error	1.0

Table 3. Systematic Errors for the 1998 run. The 1999 systematic error is about half a ppm.

The first and most important step in the analysis is forming positron times and energies from the waveform record. The algorithm agreed to is fast, reliable, stable, and largely insensitive to background. Its deadtime is less than 3 ns and, by itself, contributes nothing to the systematic error.

Excellent timing stability is required of the electronics. In particular, the average measured time must be stable to 20 ps over the first 200 μs of data-taking. For closely related reasons, the gain must be stable to 0.2 percent over the same period. Using our laser calibration system, and for gain stability, the positron energy data itself, it has been demonstrated that both goals have been met.

At high rates, which come early in the data-taking cycle, pulse pileup is also a problem. Smaller pulses which follow close on the heels of a larger trigger pulse can be missed. Two small pulses which lie directly on top of one another can masquerade as a single high energy pulse. Because pileup occurs more often at early times than later on, it can produce a systematic error in ω_a, just like a shift in gain. In our 1998 analysis, pileup was the largest single systematic error. Since then, careful studies of our pulse and precession fitting procedures have made it possible to model and correct for the effect of pileup on ω_a.

For the past year, the systematic problems associated with fitting the $(g-2)$ precession to multi-parameter functions, have been investigated by a number of collaborators. Extensions of the classic 5-parameter function described above which include such effects as pileup, fast rotation and coherent betatron oscillations have been studied, and a consistent picture is emerging from the different analyses.

5 Results and Conclusions

We now have $\sim 10^{10}$ high-energy μ^+ decay positrons on tape (~ 5 terabytes of data), which we expect to give a statistical precision of $\sim \pm 0.5$ ppm. The CERN group observed the equivalent of about 4×10^7 of our high-energy events, which came from a data sample of a total of 1.4×10^8 detected positrons of all energies. We have now reported two new measurements of $(g-2)$[10,11] and these results are shown graphically below in Fig. 10, along with the CERN results. Two large data sets are on tape from our 1999 and 2000 runs. Analysis of the 1999 data should be completed by the end of 2000, with a total error of ~ 1.4 ppm. The 2000 data should yield a statistical error of ~ 0.6 ppm.

After many years of construction and several years of engineering runs, the $(g-2)$ experiment has reached full maturity. A significant improvement on the 7.5 ppm result has now been published. With the world average one standard deviation above the standard model value, there is ample opportunity for the 1.4 ppm result to either agree with the standard model value, or be 4 standard deviations away, and <u>still</u> agree with all previous measurements.

I wish to acknowledge the many contributions made by my collaborators in $(g-2)$ in getting us to this point. This document is descended from a grant proposal written with my colleagues Jim Miller and Rob Carey, and I wish to thank them for letting me use it as the starting point for this manuscript, and for their comments. I also wish

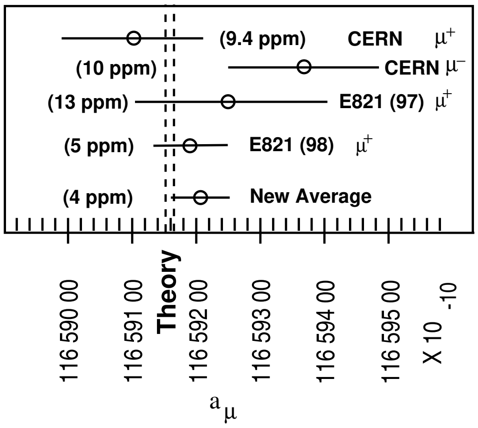

Fig. 10. Summary of the precise measurements of a_μ. The dashed lines show the standard model value.

to thank Ivan Kronkvist, Ernst Sichtermann, and Yannis Semertzidis of the $(g-2)$ publications committee for helpful comments. This work was supported in part by the U.S. Department of Energy, the U.S. National Science Foundation, the German Bundesminister für Bildung und Forschung, The Russian Ministry of Science and the US-Japan Agreement in High Energy Physics.

References

[1] H.N. Brown[2], G. Bunce[2], R.M. Carey[1], P. Cushman[10], G.T. Danby[2], P.T. Debevec[7], H. Deng[12], W.Deninger[7], S.K. Dhawan[12], V.P. Druzhinin[3], L. Duong[10], W. Earle[1], E. Efstathiadis[1], F.J.M. Farley[12], G.V. Fedotovich[3], S. Giron[10], F. Gray[7], M. Grosse-Perdekamp[12], A. Grossmann[6], U. Haeberlen[8], M.F. Hare[1], E.S. Hazen[1], D.W. Hertzog[7], V.W. Hughes[12], M. Iwasaki[11], K. Jungmann[6], D. Kawall[12] M. Kawamura[11], B.I. Khazin[3], J. Kindem[10], F. Krienen[1], I. Kronkvist[10], R. Larsen[2], Y.Y. Lee[2], I. Logashenko[1,3], R. McNabb[10], W. Meng[2], J. Mi[2], J.P. Miller[1], W.M. Morse[2], C.J.G. Onderwater[7], Y. Orlov[4], C. Özben[2], C. Pai[2], J.M. Paley[1], C. Polly[7], J. Pretz[12], R. Prigl[2], G. zu Putlitz[6], S.I. Redin[12], O. Rind[1], B.L. Roberts[1], N. Ryskulov[3], S. Sedykh[7], Y.K. Semertzidis[2], Yu.M. Shatunov[3], E. Solodov[3], M. Sossong[7], A. Steinmetz[12], L.R. Sulak[1], C. Timmermans[10], A. Trofimov[1], D. Urner[7], P. von Walter[6], D. Warburton[2], D. Winn[5], A. Yamamoto[9], D. Zimmerman[10]; [1]Department of Physics, Boston University, Boston, MA

02215, USA, [2]Brookhaven National Laboratory, Upton, NY 11973, USA, [3]Budker Institute of Nuclear Physics, Novosibirsk, Russia, [4]Newman Laboratory, Cornell University, Ithaca NY 14853, USA, [5]Fairfield University, Fairfield, CT 06430, USA, [6]Physikalisches Institut der Universität Heidelberg, 69120 Heidelberg, Germany, [7]Department of Physics, University of Illinois at Urbana-Champaign, IL 61801, USA, [8]MPI für Med. Forschung, 69120 Heidelberg, Germany, [9]KEK, High Energy Accelerator Research Organization,Tsukuba, Ibaraki 305-0801, Japan, [10]Department of Physics, University of Minnesota, Minneapolis, MN 55455, USA, [11]Tokyo Institute of Technology, Tokyo, Japan, [12]Department of Physics, Yale University, New Haven, CT 06511, USA.

[2] J. Schwinger, Phys. Rev. **73**, 416(1948), and and Phys. Rev. **75**, 898(1949)

[3] See the review by V.W. Hughes and T. Kinoshita, Rev. Mod. Phys. **71**,S133(1999) for a discussion of both the muon and electron g-factors

[4] The earlier reivew of these calculations given in T. Kinoshita, *Quantum Electrodynamics* (Directions in High Energy Physics, Vol. 7), T. Kinoshita ed., World Scientific 1990, p. 218, is also useful

[5] R.S. Van Dyck, Jr., P. Schwinberg, and H. Dehmelt, Phys. Rev. Lett. **59** (1987) 26 and in *Quantum Electrodynamics*, T. Kinoshita ed., World Scientific, 1990, p. 322

[6] G. Charpak, F.J.M. Farley, R.L. Garwin, T. Muller, J.C. Sens and A. Zichichi, Nuovo Cim. **37** (1965) 1241

[7] J. Bailey, W. Bartl, B. von Bochmann, R.C.A. Brown, F.J.M. Farley, M. Giesch, H. Jöstlein, S. van der Meer, E. Picasso and R.W. Williams, Nuovo Cim. **9A** (1972) 369

[8] J. Bailey, K. Borer, F. Combley, H. Drumm, C. Eck, F.J.M. Farley, J.H. Field, W. Flegel, P.M. Hattersley, F. Krienen, F. Lange, G. Lebée, E. McMillan, G. Petrucci, E.Picasso, O. Runolfsson, W. von Rüden, R.W. Williams and S. Wojcicki, Nucl. Phys. **B150** 1 (1979)

[9] T. Kinoshita and W.J. Marciano in *Quantum Electrodynamics* (Directions in High Energy Physics, Vol. 7), T. Kinoshita ed., World Scientific 1990, p. 419

[10] R.M. Carey et al., $(g-2)$ Collaboration, Phys. Rev. Lett. **82**, 1632 (1999).

[11] H.N. Brown, et al., $(g-2)$ Collaboration, Phys. Rev. **D62**, 091101(2000) and http://xxx.lanl.gov/archive/hep-ex paper hep-ex/0009029.

[12] S. Eidelman and F. Jegerlehner, Z. Phys., **C67** (1995) 585

[13] W.A. Worstell and D.H. Brown, (1996), Phys. Rev. **D54** 3237 (1996), and Muon (g-2) technical note # 220 (1995)

[14] M. Davier and A. Höcker, Phys. Lett. **B435**, 427(1998) and ref. therein

[15] Bernd Krause, Phys. Lett. **B390**, 392(1997)

[16] M. Hayakawa and T. Kinoshita, Phys. Rev. **D57**, 465(1998) and ref. therein.

[17] J. Bijnens, E. Pallante and J. Prades, Nucl. Phys. **B474**, 379(1996) and ref. therein.

[18] W.A. Bardeen, R. Gastmans and B Lautrup, Nucl. Phys. **B46** (1972) 319; R. Jackiw and S. Weinberg, Phys. Rev. **D5** (1972) 157; I. Bars and M. Yoshimura, Phys. Rev. **D6** (1972) 374

[19] A. Czarnecki, B. Krause and W.J. Marciano, Phys. Rev. **D52** (1995) R2619

[20] S. Peris, M. Perrottet and E. de Rafael, Phys. Lett. **B355**, 523(1995)

[21] A. Czarnecki, B. Krause and W.J. Marciano, Phys. Rev. Lett. **76** (1996) 3267

[22] T. Kinoshita, Phys. Rev. Lett. **75** (1995) 4728

[23] G. Degrassi and G.F. Giudice, Phys. Rev. **D58**, 53007(1998)

[24] A. Czarnecki and W. Marciano, *Lepton anomalous magnetic moments - a theory update*, Nucl. Phys. **S76**,245,1999, and references therein

[25] S. Brodsky and S. Drell, Phys. Rev. **D22**, 2236 (1980)

[26] G. Couture and H. Konig, Phys. Rev. **D53**, 555 (1996)

[27] F. Renard, et al., Phys. Lett. **B409**, 398 (1997)

[28] V. Bargmann, L. Michel and V.L. Telegdi, Phys. Rev. Lett. **2** (1959) 435, are generally given credit for this formula. As noted by J.D. Jackson in *Classical Electrodynamics*, (John Wiley & Sons, New York, 1975), p. 556, Thomas published an equivalent equation in 1927.

[29] G.D. Danby, et al. ($(g-2)$ collaboration), Nucl. Instrum. Meth., in press (2000)

[30] LORAN-C User's Handbook, 1992, Superintendent of Documents, U.S. Government Printing Office #050-012-00331-9.

[31] S. Sedykh, et al., *Nucl. Instrum. Methods*, in press (2000).

[32] F.J.M. Farley and E. Picasso in *Quantum Electrodynamics*, ed. T. Kinoshita, (World Scientific, Singapore, 1990), p. 479

[33] See Helmut Wiedemann, *Particle Accelerator Physics* V. 1, Springer-Verlag, 1993, p. 54 for a discussion of the weak focusing betatron.

[34] F. Combley and E. Picasso, Phys. Reports **C14**, 1 (1974).

[35] F. Krienen, D. Loomba and W. Meng, Nucl. Inst. and Met. **A283**51989.

[36] Vector Fields Limited, 24 Bankside, Kidlington, Oxford OX5 1JE, England.

[37] Muon $(g-2)$ note #286 *The* $(g-2)$ *Muon Kicker: Design and Status*, E. Efstathiadis et al., (1997) and E. Efstathiadis et al., *The Muon* $(g-2)$ *Muon Kicker*, to be submitted to *Nucl. Instrum. Methods*.

[38] W. Liu, et al., Phys. Rev. Lett. **82**, 711(1999).

[39] Particle Data Group, Eu. Phys. J. **C15**, 1 (2000).